



Energetics of the exchangeable quinone, Q_B , in Photosystem II

Sven De Causmaecker^a, Jeffrey S. Dougllass^a, Andrea Fantuzzi^a, Wolfgang Nitschke^b, and A. William Rutherford^{a,1}

^aDepartment of Life Sciences, Imperial College London, SW7 2AZ London, United Kingdom; and ^bBioénergétique et Ingénierie des Protéines/UMR 7281, Aix Marseille University, CNRS, Marseille Cedex 09 13402, France

Edited by Krishna K. Niyogi, University of California, Berkeley, CA, and approved August 13, 2019 (received for review June 25, 2019)

Photosystem II (PSII), the light-driven water/plastoquinone photo-oxidoreductase, is of central importance in the planetary energy cycle. The product of the reaction, plastoquinone (PQH₂), is released into the membrane from the Q_B site, where it is formed. A plastoquinone (PQ) from the membrane pool then binds into the Q_B site. Despite their functional importance, the thermodynamic properties of the PQ in the Q_B site, Q_B , in its different redox forms have received relatively little attention. Here we report the midpoint potentials (E_m) of Q_B in PSII from *Thermosynechococcus elongatus* using electron paramagnetic resonance (EPR) spectroscopy: $E_m(Q_B/Q_B^{\bullet-}) \approx 90$ mV, and $E_m(Q_B^{\bullet-}/Q_BH_2) \approx 40$ mV. These data allow the following conclusions: 1) The semiquinone, $Q_B^{\bullet-}$, is stabilized thermodynamically; 2) the resulting $E_m(Q_B/Q_BH_2)$ (~65 mV) is lower than the $E_m(PQ/PQH_2)$ (~117 mV), and the difference ($\Delta E \approx 50$ mV) represents the driving force for Q_BH_2 release into the pool; 3) PQ is ~50× more tightly bound than PQH₂; and 4) the difference between the $E_m(Q_B/Q_B^{\bullet-})$ measured here and the $E_m(Q_A/Q_A^{\bullet-})$ from the literature is ~234 meV, in principle corresponding to the driving force for electron transfer from $Q_A^{\bullet-}$ to Q_B . The pH dependence of the thermoluminescence associated with $Q_B^{\bullet-}$ provided a functional estimate for this energy gap and gave a similar value (≥ 180 meV). These estimates are larger than the generally accepted value (~70 meV), and this is discussed. The energetics of Q_B in PSII are comparable to those in the homologous purple bacterial reaction center.

photosynthesis | redox potential | proton-coupled electron transfer | photoinhibition

In photosynthesis, light is absorbed by chlorophyll, resulting in charge separation within a photosynthetic reaction center. In Photosystem II (PSII), the water/plastoquinone photo-oxidoreductase, the electron hole is transferred from the chlorophyll cation radical, $P_{D1}^{\bullet+}$, via a redox-active tyrosine (Tyr_Z) to the Mn_4O_5Ca cluster. After 4 sequential photochemical turnovers and the resulting oxidations of the Mn_4O_5Ca cluster (S_{0-4}), 2 water molecules are oxidized (1). On the electron acceptor side, the electron is transferred from the pheophytin anion ($Pheo_{D1}^{\bullet-}$) via a nonexchangeable plastoquinone (Q_A), which acts as a one-electron relay, to an exchangeable plastoquinone (Q_B), the terminal electron acceptor (2).

$Q_B^{\bullet-}$ decays in tens of seconds by charge recombination with S_2 or S_3 when present, but is stable for several hours if S_0 or S_1 are present (3). During the subsequent photochemical turnover, $Q_B^{\bullet-}$ accepts a second electron from the newly formed $Q_A^{\bullet-}$. This is accompanied by the 2 protonation steps, thought to occur sequentially, one before and one after the arrival of the second electron (4), as occurs in the homologous site in purple bacteria (5). The Q_BH_2 formed is released from the site and enters the PQ/PQH₂ pool, from where it can deliver electrons to the cytochrome *b₆f* complex (6–8).

Due to the 2-electron chemistry of Q_B , the $Q_B^{\bullet-}$ state is the only state on the electron acceptor side that cannot be stabilized by forward electron transfer; i.e., there is no “kinetic control” on this step (9). “Kinetic control” of electron transfer occurs in photosynthetic reaction centers when the forward rate outruns both the backward rate and the charge pair recombination rate (9). As a stable intermediate, $Q_B^{\bullet-}$ is therefore available to back-react via $Q_A^{\bullet-}$ with the S_2 and S_3 states on the donor side (3). Two main

competing back-reaction pathways occur within PSII: 1) the direct route via electron tunneling from $Q_A^{\bullet-}$ to $P^{\bullet+}$ and 2) the indirect route via thermal repopulation of the $P^{\bullet+}Pheo_{D1}^{\bullet-}$ state (10). Recombination from the $P^{\bullet+}Pheo_{D1}^{\bullet-}$ state mainly forms the chlorophyll triplet state $^3P_{680}$ (11), which reacts with oxygen to form highly reactive and damaging singlet oxygen 1O_2 (12).

The driving force (ΔG) for electron transfer between Q_A and Q_B determines the $Q_A^{\bullet-}Q_B \leftrightarrow Q_AQ_B^{\bullet-}$ equilibrium and therefore the extent to which back-reactions from $Q_B^{\bullet-}$ (or Q_BH_2) to Q_A can occur. This equilibrium is determined by the difference between the midpoint potentials (E_m) of the donor and the acceptor, $E_m(Q_A/Q_A^{\bullet-})$ and $E_m(Q_B/Q_B^{\bullet-})$ or $E_m(Q_B^{\bullet-}/Q_BH_2)$, according to the following equation:

$$\Delta G = -nF(\Delta E). \quad [1]$$

The redox state of Q_A can be monitored relatively easily using fluorescence measurements. $Q_A^{\bullet-}$ has an electrostatic effect on the potential of $Pheo_{D1}/Pheo_{D1}^{\bullet-}$, decreasing the already small energy gap between P^* (the primary donor) and the first radical pair, which results in a decrease in the yield of charge separation and an increase in fluorescence. A wide range of values have been reported (13). This scatter of reported values is, at least in part, due to the potential being modulated to regulate forward and particularly back electron transfer reactions (9). The Q_A redox potential is affected by the binding of the Mn_4O_5Ca cluster to its site (10, 13–15) and by the bicarbonate binding to the nonheme iron (16) (Fig. 1). The redox potential of the $Q_A/Q_A^{\bullet-}$ couple in the fully functional, bicarbonate-bound system is –144 mV (15, 16).

Significance

The E_m values of the 2 Q_B redox couples, $E_m(Q_B/Q_B^{\bullet-})$ and $E_m(Q_B^{\bullet-}/Q_BH_2)$, in Photosystem II are fundamental for understanding the enzyme function, but they remain vague. Using EPR signals arising from the semiquinone, $Q_B^{\bullet-}$, we have now measured both redox couples. The semiquinone is thermodynamically stable and has a relatively high potential. This minimizes back-reactions and electrons leaking onto O_2 , explaining the remarkable stability of $Q_B^{\bullet-}$. The release of Q_BH_2 is thermodynamically favorable, and the binding of the substrate PQ is greatly favored over the product PQH₂. This optimizes PSII function in the presence of a largely reduced plastoquinone pool. This work corrects and explains a recent report of anomalous values for the Q_B redox couples.

Author contributions: A.W.R. designed research; S.D.C., J.S.D., W.N., and A.W.R. performed research; S.D.C. designed and built the thermoluminescence instrument; S.D.C., A.F., W.N., and A.W.R. analyzed data; and S.D.C., A.F., W.N., and A.W.R. wrote the paper. The authors declare no conflict of interest.

This article is a PNAS Direct Submission.

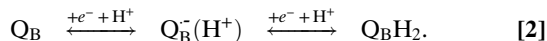
Published under the PNAS license.

¹To whom correspondence may be addressed. Email: a.rutherford@imperial.ac.uk.

This article contains supporting information online at www.pnas.org/lookup/suppl/doi:10.1073/pnas.1910675116/-DCSupplemental.

First published September 5, 2019.

The measurement of the redox state of Q_B is more complicated than that of Q_A . Firstly, there is no easy experimental probe for the redox state of Q_B . Secondly, in contrast to Q_A , which undergoes a one-electron redox reaction forming $Q_A^{\bullet-}$ without the involvement of protons, the Q_B reduction involves 2 electrons and 2 protons (Eq. 2).



Thirdly, Q_A is a tightly bound cofactor in both of its redox states, while Q_B has 2 of the 3 relevant redox states (Q_B and Q_BH_2) that are relatively weakly bound and exchangeable with PQ or PQH₂. As a consequence, kinetic data have been used to estimate the redox potential of Q_B by deriving the apparent equilibrium constant, K , for the electron transfer between $Q_A^{\bullet-}$ and Q_B (17–19). Taking K as 15 ($K = 10$ to 20 in refs. 17–19), the energy gap is 70 meV, so, with the E_m of $Q_A/Q_A^{\bullet-}$ of -144 mV (15, 16), the E_m of $Q_B/Q_B^{\bullet-}$ E_m would thus be -74 mV (17–19). Due to the complex nature of the experiments from which the kinetic parameters were extracted, uncertainties remain (17–20). A theoretical model based on thermoluminescence (TL) was used to obtain a similar value for the energy gap between the $Q_A/Q_A^{\bullet-}$ and $Q_B/Q_B^{\bullet-}$ couples (21, 22). Doubts remain, however, as experimental observables in TL do not always fit with thermodynamic parameters derived from the TL model (21, 23).

In summary, the mechanism and energetics of the PSII acceptor side and especially Q_B are still relatively poorly understood. The redox potentials for the 2 couples, $E_m(Q_B/Q_B^{\bullet-})$ and $E_m(Q_B^{\bullet-}/Q_BH_2)$, have received relatively little attention, despite being central to understanding the quinone reduction function of this enzyme. These redox potentials should provide thermodynamic information related to 1) the stability of the electron transfer intermediates and their tendency to back-react, or to react with O_2 ; 2) the driving force for forward reactions; and 3) the (de)binding properties of the substrate (PQ) and product (PQH₂).

An experimental estimate of the E_m values of the 2 Q_B redox couples, $Q_B/Q_B^{\bullet-}$ and $Q_B^{\bullet-}/Q_BH_2$, based on equilibrium redox titrations was published recently (24). Fourier transform infrared (FTIR) was used to monitor $Q_B^{\bullet-}$ formation upon illumination by a single flash as a function of the applied potential. The data seemed to show that $Q_B^{\bullet-}$ was not thermodynamically stable, a surprising result in light of the mechanistic implications and given the conflicting results in the homologous purple bacterial reaction centers (20, 25–27).

Here we have used electron paramagnetic resonance (EPR) spectroscopy to estimate the redox potential of the 2 couples, $Q_B/Q_B^{\bullet-}$ and $Q_B^{\bullet-}/Q_BH_2$. Two different EPR signals were measured: a

$Q_B^{\bullet-}Fe^{2+}$ semiquinone signal (28) and a $Q_A^{\bullet-}Fe^{2+}Q_B^{\bullet-}$ biradical signal (29, 30). We also used TL to estimate empirically the energy gap between the $Q_A/Q_A^{\bullet-}$ and $Q_B/Q_B^{\bullet-}$ couples, without relying on the theoretical model previously employed. Our results differ from previous measurements and estimates and show that the semiquinone, $Q_B^{\bullet-}$, is stabilized thermodynamically and that the plastoquinone is preferentially bound compared to the plastoquinol.

Results

EPR spectra of PSII were measured at a series of electrode potentials. The D2-Y160F mutant lacking tyrosine D (Tyr_D) was used to eliminate the Tyr_D[•] signal, which would otherwise dominate the PSII EPR spectrum in the radical region (31). At each potential, dark spectra and spectra after illumination at 77 K were recorded. Fig. 2A shows a scan of the radical region around $g = 2$. The appearance and disappearance of the EPR signal as a function of potential can be observed. This signal has been assigned to the low-field edge of the ground-state doublet of the semiquinone, $Q_B^{\bullet-}Fe^{2+}$ (28).

Fig. 2B shows a full spectrum scan of the same samples as used in Fig. 2A after illumination at 77 K. A peak at 4,000 G ($g = 1.66$) shows a potential dependence similar to that of the $Q_B^{\bullet-}Fe^{2+}$ signal. The $g = 1.66$ signal has been assigned to the $Q_A^{\bullet-}Fe^{2+}Q_B^{\bullet-}$ biradical state (29, 30). The low-temperature illumination generates $Q_A^{\bullet-}$ in nearly all of the centers. No electron transfer occurs from $Q_A^{\bullet-}$ to Q_B or to $Q_B^{\bullet-}$ at 77 K (30); therefore the biradical signal should only be observed if $Q_B^{\bullet-}$ were present before the 77-K illumination. Thus, the biradical signal can be used to monitor the presence of $Q_B^{\bullet-}$ independently of the $Q_B^{\bullet-}Fe^{2+}$ signal.

To assess the proportion of $Q_B^{\bullet-}$ formed during the titration, the signal size of the $Q_B^{\bullet-}Fe^{2+}$ signal if present in 100% of the centers was estimated. In a dark-adapted sample, $Q_B^{\bullet-}$ is present in ~40% of the centers, while Q_B is present in the rest (3, 30). That proportionality can be inverted by illuminating at 77 K and subsequently thawing in darkness (3). Therefore, the sum of the amplitudes of the signals present before and after this treatment should yield the size of the signal when $Q_B^{\bullet-}$ is present in all of the centers. This experiment was done, and the estimated value for 100% $Q_B^{\bullet-}$ was used to calibrate the amplitudes of the EPR signals in the titrations (SI Appendix, Fig. S2).

Fig. 3 shows a plot of the normalized $Q_B^{\bullet-}Fe^{2+}$ and $Q_A^{\bullet-}Fe^{2+}Q_B^{\bullet-}$ signals versus the measured potential, combining data from 3 individual titrations (including those in Fig. 2). Titrations were carried out in oxidizing and reducing directions. Due to poor mediation between ~0 mV and 50 mV, fewer reliable data points could be collected in that region, and the data are more scattered. The maximum amplitude, which occurs at 67 mV, represented about 55% of the centers in the stable $Q_B^{\bullet-}$ state. Data were fitted using the model first established by Michaelis (32). The resulting potentials for the 2 couples were $E_m(Q_B/Q_B^{\bullet-}) = 92 \pm 23$ mV and $E_m(Q_B^{\bullet-}/Q_BH_2) = 43 \pm 23$ mV.

The retention of the Mn₄O₅Ca cluster during the course of the titration was verified in 2 ways: firstly, by the presence of free “hexaquo” Mn²⁺ signals in the spectra, representing a loss of the Mn₄O₅Ca cluster, and, secondly, by the ability to form the S₂ multiline signal (33). The Mn₄O₅Ca cluster was retained in the majority of centers even after exposure to low potentials (SI Appendix, Fig. S5 and associated text).

In addition to the redox titrations of the EPR signals associated with $Q_B^{\bullet-}$, pH-dependent TL measurements were used to estimate the energy gap between the $Q_A/Q_A^{\bullet-}$ and $Q_B/Q_B^{\bullet-}$ couples in PSII cores containing TyrD. TL measures the emission of luminescence associated with the heating-induced back-reaction of a stable charge-separated state. The peak temperature of TL is indicative of the energy stored in the charge-separated state and is determined by redox potentials of both the recombination partners, in this case, S₂/S₁ and $Q_B/Q_B^{\bullet-}$ (3, 21). Below pH of ~7, the S₂/S₁ couple involves very little protonation and is almost independent of pH (34). The $Q_B/Q_B^{\bullet-}$ couple involves proton release when $Q_B^{\bullet-}$ is reoxidized and is expected to follow Nernst behavior (19, 35, 36), with the redox potential changing by -59 mV per pH unit. Thus, the pH dependence of the S₂ $Q_B^{\bullet-}$

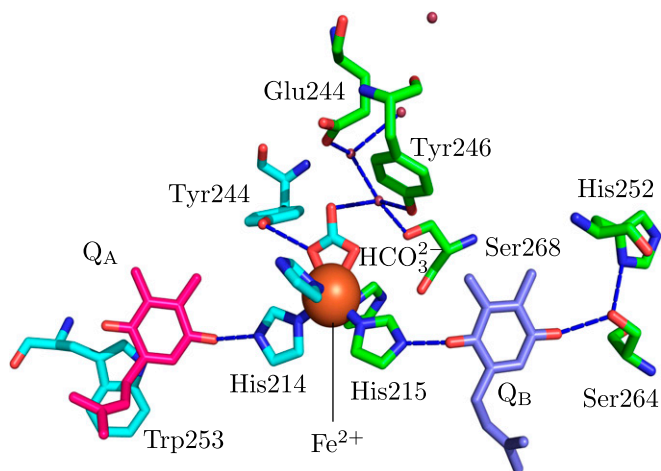


Fig. 1. PSII acceptor side. Blue lines denote possible hydrogen bonds. Data from the 1.9-Å crystal structure (Protein Data Bank ID Code 3WU2) (53).

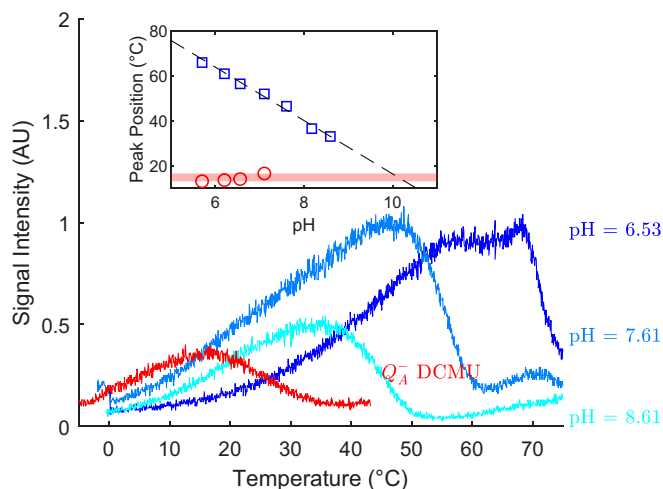


Fig. 4. Thermoluminescence of long-dark-adapted PSII cores from *T. elongatus*. Blue, after one saturating flash at different values of pH; red, after the addition of DCMU. Inset shows a plot of the $S_2Q_B^{\bullet-}$ peak position versus the pH with a slope of $-11.6\text{ }^\circ\text{C/pH}$ unit and a plot of the $S_2Q_B^{\bullet-}$ peak over the restricted zone of pH in which it is pH independent. At pH 6.5, a TL band of $\sim 70\text{ }^\circ\text{C}$ becomes the dominant emission but is not attributed to the $S_2Q_B^{\bullet-}$; it is more likely to be from the so-called C band (54).

site, with larger values equating to a more stable semiquinone. When titrating a free quinone in the membrane, the semiquinone is not stabilized, the redox transition occurs as a steeper $n = 2$ curve (i.e., a 2-electron transition), no semiquinone can be observed, and the ΔE_m is negative. Although the membrane is aprotic, the quinone head group can access the aqueous solvent, and thus the semiquinone is destabilized [$\Delta E_m \approx -500\text{ meV}$ for ubiquinone (39)]. Our data indicate that $Q_B^{\bullet-}$ is strongly bound and stabilized by the Q_B site in comparison to a quinone in the membrane. The structure of the Q_B site (Fig. 1) shows several features that likely contribute to the electrochemical properties of $Q_B^{\bullet-}$, including 1) the proximity to the nonheme ferrous iron, 2) hydrogen bonds from $D_1\text{His}215$ and $D_1\text{Ser}264$ to both carbonyls of the quinone, and 3) the likely protonation of the distal H-bonding $D_1\text{Ser}264/\text{His}252$ pair (4).

This stabilization can be rationalized in part as a damage prevention mechanism. In PSII, back-reactions from $P^+Q_A^{\bullet-}$ result in damage to the complex (9, 16). A large gap between the $Q_A/Q_A^{\bullet-}$ and $Q_B/Q_B^{\bullet-}$ couples would favor Q_B reduction and lower the equilibrium concentration of $Q_A^{\bullet-}$, thereby diminishing the likelihood of a damaging back-reaction from $Q_A^{\bullet-}$. This stabilization of the semiquinone would come at a cost, because a more positive $E_m(Q_B/Q_B^{\bullet-})$ must yield a more negative $E_m(Q_B^{\bullet-}/Q_BH_2)$ in order to maintain the chemical requirement that the average E_m for the 2 couples remains unchanged (see below). Back-reactions from the fully reduced quinol, Q_BH_2 , to Q_A would therefore become more likely. These back-reactions, however, would only occur when the plastoquinone pool is reduced, because quinol/quinone exchange occurs orders of magnitude faster ($\sim 10\text{ ms}$; ref. 40) than the $S_2Q_BH_2$ back-reaction, which we predict to decay with kinetics between the recombination rates of $Q_A^{\bullet-}$ and $Q_B^{\bullet-}$ with S_2 [i.e., between $\sim 1\text{ s}$ and $\sim 30\text{ s}$ (41)].

The high potential E_m ($\sim 90\text{ mV}$) for the $Q_B/Q_B^{\bullet-}$ also means that $Q_B^{\bullet-}$ is a poor reductant for O_2 forming superoxide ($E_m(O_2/O_2^{\bullet-}) \approx -160\text{ mV}$). It has been suggested that $Q_B^{\bullet-}$ may be a source of reactive oxygen species (42); however, its very long lifetime, with half-times of hours in the presence of S_1 and S_0 (3, 30), argues against this. The present work showing the thermodynamic stabilization of $Q_B^{\bullet-}$ provides a good explanation for its lack of reactivity with oxygen and for its very long lifetime in the dark.

The presence of a stabilized $Q_B^{\bullet-}$ directly contradicts a recent report (24) (discussed in detail below) but is supported by other reports. A reductive titration of the $g = 1.66$ biradical signal with

PSII particles from *Phormidium laminosum* was reported previously as part of the work done to identify the origin of the biradical signal (29). Although no reversibility was demonstrated and the signal size was not quantified, a thermodynamically stable $Q_B^{\bullet-}$, similar to that reported in this work, was clearly present in the reductive titration.

A thermodynamically stable $Q_B^{\bullet-}$ was also present in the homologous purple bacterial reaction centers from *Rhodobacter sphaeroides* (25), *Chromatium vinosum* (26), and *Blastochloris viridis* (27). These titrations show ~ 30 to 50% of the total quinone form as a stable semiquinone (see *SI Appendix, Fig. S7* for a corrected fitting of these titrations). The exact ΔE_m and E_m^{avg} all differ from each other to some extent, perhaps reflecting different mechanistic requirements in the different species, but, in all reaction centers, the semiquinone, $Q_B^{\bullet-}$, is clearly thermodynamically stabilized. Together, these studies in the literature (25–27, 29) provide strong support for the current results.

Preferential Binding of the Quinone vs. the Quinol. Although the redox potential of the plastoquinone in the pool from *T. elongatus* has not been measured, it is expected to be very similar to that in other organisms, i.e., a 2-electron transition at 117 mV (43, 44). The average for the 2 Q_B redox couples measured here ($E_m^{\text{avg}} \approx 65\text{ mV}$) is therefore about 50 mV lower than that of the plastoquinone pool. This represents a significant driving force for the release of the PQH_2 to the pool. This should be considered as an additional energy loss in the ongoing effort to understand energy use in PSII. A smaller but qualitatively similar energy loss was reported earlier for UQH_2 release from the Q_B site in the purple bacterial reaction center to the pool, based on a computational chemistry approach (39).

From the difference in redox potential, the ratio of the binding constants for the quinone and the quinol forms can be calculated (16) (see *SI Appendix, Fig. S6* and associated text for details). It is found that the quinone is bound to the Q_B site ~ 50 times more tightly than the quinol. Again, this fits qualitatively with the situation reported in purple bacterial reaction centers (39, 45). For PSII to function optimally, it makes sense that the binding of the substrate (the quinone) is favored over that of the product (the quinol). Preferential quinone binding will allow PSII to function when the pool is significantly reduced.

In the literature, it has often been assumed that the binding constants of the quinone and quinol in the Q_B site are equal both in PSII and in purple bacterial reaction centers (e.g., refs. 18 and 20). Nevertheless, the $Q_B^{\bullet-}$ redox titrations in purple bacterial reaction centers indicated the preferential binding of the quinone over the quinol (25), and other reports favor this binding regime (6, 46), partly because of the experimental indications (25–27, 39) and partly because it seemed mechanistically more likely [see *SI Appendix* for further discussion and a possible exception in *C. vinosum* (26)]. The present work is good experimental evidence for preferential binding of the quinone over the quinol in PSII.

The Difference in Redox Potentials Between Q_A and Q_B . The difference in equilibrium redox potentials between the $Q_A/Q_A^{\bullet-}$ and $Q_B/Q_B^{\bullet-}$ couples reported here, $\sim 234\text{ meV}$, is larger than previously estimated ($\sim 70\text{ meV}$) from the kinetics of the forward and backward electron transfer reactions between Q_A and Q_B (21, 41). The following factors could contribute to the mismatch: 1) The previous dynamic measurements are based on assumptions that may be complicated by the so-called “gating effect,” which determines the rate-limiting step of electron transfer between Q_A and Q_B rather than the driving force (47). This dynamic effect is not accounted for in the previous estimates and may at least contribute to the discrepancy. 2) While the Q_B redox couples themselves do not suffer from the problem of being titrated adjacent to an already reduced cofactor, the E_m of $Q_A/Q_A^{\bullet-}$ may be systematically underestimated (a lower potential) in redox titrations due to the binding of Q_BH_2 which would result in a smaller energy gap. 3) The $Q_A/Q_A^{\bullet-}$ couple may be more specifically sensitive to modulation from the electron donor side, which would also affect the energy gap estimate (see *SI Appendix* for a more detailed discussion).

Given the uncertainty about the energy gap between the E_m $Q_A/Q_A^{\bullet-}$ from the literature and the $E_m Q_B/Q_B^{\bullet-}$ measured here, we made an independent estimate of this energy gap by estimating empirically the energy gap between $S_2Q_A^{\bullet-}$ and $S_2Q_B^{\bullet-}$ as a function of pH. It was assumed that the energy gap determining the peak position of the TL follows Nernst behavior and shifts by 59 mV per pH unit. This assumption seems justified given the experimentally determined proton stoichiometries in the literature (34, 36). The resulting value, ~ 180 meV or ~ 230 meV if we assume a DCMU binding effect (40), is similar to the energy gap obtained from the equilibrium redox titrations (~ 234 meV). A similar value (~ 212 meV) is obtained by using the data from Vass and Inoue (37). This estimate is done in the presence of S_2 (as were the previous kinetic estimates) rather than S_1 (as were the equilibrium redox titrations), thus indicating the absence of a significant influence of the S state on the energy gap. We remain somewhat skeptical about the similarity of the 2 values because in the TL method: 1) The determination of the $S_2Q_A^{\bullet-}$ and $S_2Q_B^{\bullet-}$ peak temperatures are not very accurate, and 2) the added DCMU shift of 50 mV has not yet been determined in PSII cores from *T. elongatus*. Despite these shortcomings, the TL measurements seem to provide independent support for the energy gap being significantly bigger than 70 meV estimated previously.

A large energy gap would make sense in functional terms. As $Q_B^{\bullet-}$ is the terminal electron acceptor, it cannot be prevented from back-reacting by “kinetic control,” i.e., by ensuring the forward electron transfer is faster than the back-reactions (9). Thus wasteful and damaging back-reactions can be minimized by increasing the energy gap between the $Q_A/Q_A^{\bullet-}$ and $Q_B/Q_B^{\bullet-}$ couples.

Rationalizing the Conflicting Report in the Literature. The findings in the present work differ significantly from a recently published study on the redox potentials of Q_B (24). In that work, redox titrations were performed in which the ability to form $Q_B^{\bullet-}$ by a single saturating flash was monitored by FTIR measurements in a spectroelectrochemical thin cell (24). This is not a direct measurement of $Q_B^{\bullet-}$; rather, it is a measurement of the ability to form $Q_B^{\bullet-}$ upon flash illumination (or to form Q_BH_2 if $Q_B^{\bullet-}$ were already present). This method should, in principle, provide a valid Q_B titration. The results in ref. 24, however, showed no evidence for stable $Q_B^{\bullet-}$ formation. Instead a redox curve was reported that was essentially indistinguishable from an $n = 2$ curve, i.e., a 2-electron transition, with an $E_m = 155$ mV at pH 6.5; this is equivalent to 125 mV at pH 7. The E_m and the $n = 2$ curve are both characteristic of a titration of free plastoquinone (43, 44). While the PSII cores have no membrane and thus no membrane-localized quinone pool, they do contain 1 or 2 free quinones in addition to Q_B , and these quinones act as a limited plastoquinone pool (30, 48, 49).

Here we show that the E_m values of the quinone couples in the Q_B site are more negative than that of free quinone; therefore, in a reductive titration, the free quinone will be reduced before the Q_B quinone. Since quinone exchange happens on the millisecond timescale, this free quinone will exchange with a quinone in the Q_B site, allowing the free quinone to be reduced. If the mediation with the Q_B site is insufficient, electrons will not be removed from Q_BH_2 , and therefore the redox state of the quinone in the Q_B site will reflect the redox state of the pool, irrespective of the true quinone potential in the Q_B site. Under these conditions, an $n = 2$ Nernst dependency at the E_m of the pool would be observed even when probing exclusively the Q_B site. Given that 1) only 3 mediators were used in the titration, only one of which is in the appropriate range, and 2) the flash-induced state monitored had to be stable for several minutes in order to allow the data collection, it seems likely that the redox mediation was insufficient and therefore the E_m of PQ was measured (24). See *SI Appendix* for a detailed analysis of ref. 24.

Conclusion

Fig. 5 summarizes the results of the present work and provides a consistent energetic description of PSII, now including the 2 redox potentials of the Q_B couples. This provides insights into the redox

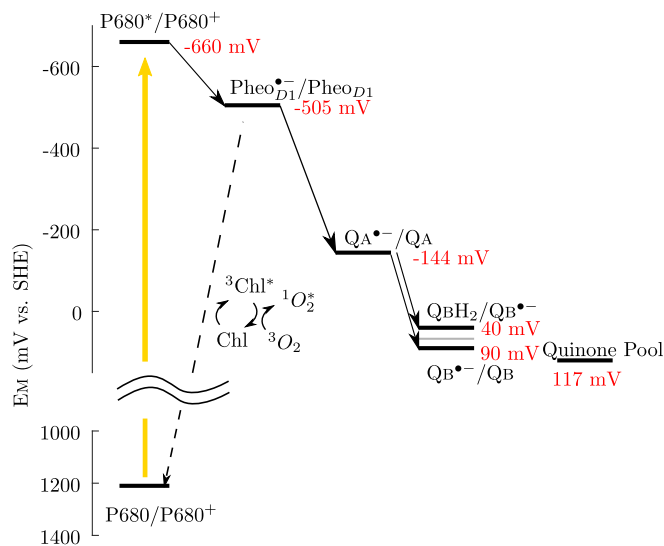


Fig. 5. Redox scheme of PSII. Redox potentials values were taken from the present work for the Q_B couples and from ref. 16 for Q_A , from ref. 55 for Pheo $_{D1}$, from ref. 2 for P680, and from refs. 43 and 44 for the quinone pool. The yellow arrow represents excitation of the P680 chlorophyll. The straight black arrows are electron transfer events. The curved arrows show excitation transfer.

tuning of Q_B with respect to the redox potentials of its neighboring redox partners, Q_A and free plastoquinone. The energy gap between the $Q_A/Q_A^{\bullet-}$ and the 2 Q_B redox couples reported here is significantly larger than previously assumed. The redox potentials need to be high enough compared to that of Q_A to provide for sufficient driving force and to minimize back-reactions. The redox potential of the plastoquinone pool limits the average value of the 2 Q_B couples. The measured value shows that, in PSII, ~ 50 meV of driving force is expended to ensure rapid debinding of the quinol and the preferential binding of the quinone. These data indicate that the protein tunes the thermodynamics of the Q_B redox chemistry to optimize function over a wide range of plastoquinone pool reduction states, while minimizing back-reactions and side reactions with O_2 .

Materials and Methods

Isolation of PSII from *T. elongatus*. PSII cores were isolated from D2-Y160F; CP43-His strain (31) using a method based on that of Sugiura and Inoue (50) with specific modifications described in *SI Appendix*.

EPR-Detected Potentiometric Titrations. Multiple PSII preparations were pooled to yield 7 mL to 10 mL of purified PSII at 0.7 mg (Chl)-mL $^{-1}$ in titration buffer. Redox titrations were carried out essentially as described by Dutton (51) at 15 °C under a bicarbonate-enriched argon atmosphere in absolute darkness and in the presence of the following redox mediators all at 50 μ M: *N,N,N,N*-tetramethyl-*p*-phenylenediamine (300 mV), 2,6-Dichlorophenolindophenol (217 mV), Phenazine methosulfate (80 mV), Thionine (64 mV), Phenazine ethosulfate (55 mV), Methylene blue (11 mV), Pycocyanin (−34 mV), Indigotrisulfonate (−46 mV), and Resorufin (−51 mV). Reductive titrations were carried out using sodium dithionite; oxidative titrations were carried out using potassium ferricyanide. EPR spectra were recorded on a Bruker ElexSys X-band spectrometer fitted with an Oxford Instruments liquid helium cryostat and temperature control system. Illumination at 77 K (20 min) was carried out in an unsilvered dewar with a halogen lamp (LQ 2600; Fiberoptic-Heim AG). See *SI Appendix*, Fig. S1 for further information on data treatment and fitting.

TL was measured using a laboratory-built apparatus (52). PSII cores (20 μ g [Chl]-mL $^{-1}$) in buffer 1 (MOPS was used instead of MES at pH > 7 and HEPES at pH > 8, 20% glycerol instead of 10%) were dark-adapted for >1 h at 4 °C, and 200- μ L samples were loaded in darkness. If required, DCMU (in ethanol) was added to the sample on the sample plate (50 μ M final concentration). The pH was measured in darkness directly prior to the experiment. Samples were cooled (<30 s) to -20 °C with liquid N_2 directly after a ~ 5 -ns laser flash at 523 nm, the second harmonic of a Nd-YAG laser (Minilite II; Continuum). The

frozen samples were then heated at a constant rate of 20 °Cmin⁻¹, and TL was detected with a photomultiplier (H7422-50; Hamamatsu). The signal was amplified using a transimpedance amplifier (C7319; Hamamatsu) and digitized using a microcontroller board based on the Atmel SAM3X8E ARM Cortex-M3 CPU (Arduino Due).

ACKNOWLEDGMENTS. We are grateful for access to the EPR facilities available at the Aix-Marseille University EPR center and at the national TGE-RPE

- H. Dau, I. Zaharieva, Principles, efficiency, and blueprint character of solar-energy conversion in photosynthetic water oxidation. *Acc. Chem. Res.* **42**, 1861–1870 (2009).
- F. Rappaport, B. A. Diner, Primary photochemistry and energetics leading to the oxidation of the (Mn)₄Ca cluster and to the evolution of molecular oxygen in photosystem II. *Coord. Chem. Rev.* **252**, 259–272 (2008).
- A. W. Rutherford, A. R. Crofts, Y. Inoue, Thermoluminescence as a probe of photosystem II photochemistry. The origin of the flash-induced glow peaks. *Biochim. Biophys. Acta Bioenerg.* **682**, 457–465 (1982).
- K. Saito, A. W. Rutherford, H. Ishikita, Mechanism of proton-coupled quinone reduction in Photosystem II. *Proc. Natl. Acad. Sci. U.S.A.* **110**, 954–959 (2013).
- C. A. Wraight, Proton and electron transfer in the acceptor quinone complex of photosynthetic reaction centers from *Rhodobacter sphaeroides*. *Front. Biosci.* **9**, 309–337 (2004).
- C. A. Wraight, Oxidation-reduction physical chemistry of the acceptor quinone complex in bacterial photosynthetic reaction centers: Evidence for a new model of herbicide activity. *Isr. J. Chem.* **21**, 348–354 (1981).
- F. Müh, C. Glöckner, J. Hellmich, A. Zouni, Light-induced quinone reduction in photosystem II. *Biochim. Biophys. Acta* **1817**, 44–65 (2012).
- T. Cardona, A. Sedoud, N. Cox, A. W. Rutherford, Charge separation in photosystem II: A comparative and evolutionary overview. *Biochim. Biophys. Acta* **1817**, 26–43 (2012).
- A. W. Rutherford, A. Osyczka, F. Rappaport, Back-reactions, short-circuits, leaks and other energy wasteful reactions in biological electron transfer: Redox tuning to survive life in O₂. *FEBS Lett.* **586**, 603–616 (2012).
- G. N. Johnson, A. W. Rutherford, A. Krieger, A change in the midpoint potential of the quinone QA in Photosystem II associated with photoactivation of oxygen evolution. *Biochim. Biophys. Acta Bioenerg.* **1229**, 202–207 (1995).
- A. W. Rutherford, D. R. Paterson, J. E. Mullett, A light-induced spin-polarized triplet detected by EPR in Photosystem II reaction centers. *Biochim. Biophys. Acta Bioenerg.* **635**, 205–214 (1981).
- J. R. Durrant, L. B. Giorgi, J. Barber, D. R. Klug, G. Porter, Characterisation of triplet states in isolated Photosystem II reaction centres: Oxygen quenching as a mechanism for photodamage. *Biochim. Biophys. Acta Bioenerg.* **1017**, 167–175 (1990).
- A. Krieger, A. W. Rutherford, G. N. Johnson, On the determination of redox midpoint potential of the primary quinone electron acceptor, QA, in Photosystem II. *Biochim. Biophys. Acta Bioenerg.* **1229**, 193–201 (1995).
- A. Krieger, E. Weis, S. Demeter, Low-pH-induced Ca²⁺-ion release in the water-splitting system is accompanied by a shift in the midpoint redox potential of the primary quinone acceptor QA. *Biochim. Biophys. Acta Bioenerg.* **1144**, 411–418 (1993).
- T. Shibamoto, Y. Kato, M. Sugiura, T. Watanabe, Redox potential of the primary plastoquinone electron acceptor Q(A) in photosystem II from *Thermosynechococcus elongatus* determined by spectroelectrochemistry. *Biochemistry* **48**, 10682–10684 (2009).
- K. Brinkert, S. De Causmaecker, A. Krieger-Liszky, A. Fantuzzi, A. W. Rutherford, Bicarbonate-induced redox tuning in Photosystem II for regulation and protection. *Proc. Natl. Acad. Sci. U.S.A.* **113**, 12144–12149 (2016).
- B. A. Diner, Dependence of the deactivation reactions of Photosystem II on the redox state of plastoquinone pool a varied under anaerobic conditions. Equilibria on the acceptor side of Photosystem II. *Biochim. Biophys. Acta Bioenerg.* **460**, 247–258 (1977).
- B. Bouges-Bocquet, “Electron acceptors of photosystem II” in *Proceedings of the 3rd International Congress on Photosynthesis*, M. Avron, Ed. (Elsevier, 1975), pp. 579–588.
- H. H. Robinson, A. R. Crofts, “Kinetics of proton uptake and the oxidation-reduction reactions of the quinone acceptor complex of PS II from pea chloroplasts” in *Proceedings of the International Congress on Photosynthesis*, Brussels, Belgium, Aug 1–6, 1983, C. Sybesma, Ed. (Martinus Nijhoff, The Hague, 1984), vol. 1, pp. 477–480.
- A. R. Crofts, C. A. Wraight, The electrochemical domain of photosynthesis. *Biochim. Biophys. Acta Bioenerg.* **726**, 149–185 (1983).
- F. Rappaport, J. Lavergne, Thermoluminescence: Theory. *Photosynth. Res.* **101**, 205–216 (2009).
- S. Rose et al., D1-arginine257 mutants (R257E, K, and Q) of *Chlamydomonas reinhardtii* have a lowered QB redox potential: Analysis of thermoluminescence and fluorescence measurements. *Photosynth. Res.* **98**, 449–468 (2008).
- Y. Kato et al., Influence of the PsaA1/PsbA3, Ca²⁺/Sr²⁺ and Cl⁻/Br⁻ exchanges on the redox potential of the primary quinone Q_A in photosystem II from *Thermosynechococcus elongatus* as revealed by spectroelectrochemistry. *Biochim. Biophys. Acta* **1817**, 1998–2004 (2012).
- Y. Kato, R. Nagao, T. Noguchi, Redox potential of the terminal quinone electron acceptor QB in photosystem II reveals the mechanism of electron transfer regulation. *Proc. Natl. Acad. Sci. U.S.A.* **113**, 620–625 (2016).
- A. W. Rutherford, M. C. W. Evans, Direct measurement of the redox potential of the primary and secondary quinone electron acceptors in *Rhodospseudomonas sphaeroides* (wild-type) by EPR spectrometry. *FEBS Lett.* **110**, 257–261 (1980).
- P. Heathcote, A. W. Rutherford, “An EPR signal arising from QB-Fe in chromatium vinosum” in *Progress in Photosynthesis Research* (Dordrecht, 1986), vol. 1, pp. 201–204.
- A. W. Rutherford, P. Heathcote, M. C. W. Evans, Electron-paramagnetic-resonance measurements of the electron-transfer components of the reaction centre of *Rhodospseudomonas viridis*. Oxidation-reduction potentials and interactions of the electron acceptors. *Biochem. J.* **182**, 515–523 (1979).
- A. Sedoud et al., Semiquinone-iron complex of photosystem II: EPR signals assigned to the low-field edge of the ground state doublet of QA•-Fe²⁺ and QB•-Fe²⁺. *Biochemistry* **50**, 6012–6021 (2011).
- A. R. Corrie, J. H. A. Nugent, M. C. W. Evans, Identification of EPR signals from the states QaQb and Qb in photosystem II from *Phormidium laminosum*. *Biochim. Biophys. Acta Bioenerg.* **1057**, 384–390 (1991).
- C. Fufezan, C. Zhang, A. Krieger-Liszky, A. W. Rutherford, Secondary quinone in photosystem II of *Thermosynechococcus elongatus*: Semiquinone-iron EPR signals and temperature dependence of electron transfer. *Biochemistry* **44**, 12780–12789 (2005).
- M. Sugiura et al., Site-directed mutagenesis of *Thermosynechococcus elongatus* photosystem II: The O₂-evolving enzyme lacking the redox-active tyrosine D. *Biochemistry* **43**, 13549–13563 (2004).
- L. Michaelis, Theory of the reversible two-step oxidation. *J. Biol. Chem.* **96**, 703–715 (1932).
- G. C. Dismukes, Y. Siderer, EPR spectroscopic observations of a manganese center associated with water oxidation in spinach chloroplasts. *FEBS Lett.* **121**, 78–80 (1980).
- F. Rappaport, J. Lavergne, Proton release during successive oxidation steps of the photosynthetic water oxidation process: Stoichiometries and pH dependence. *Biochemistry* **30**, 10004–10012 (1991).
- A. W. Rutherford, G. Renger, H. Koike, Y. Inoue, Thermoluminescence as a probe of photosystem II. The redox and protonation states of the secondary acceptor quinone and the O₂-evolving enzyme. *Biochim. Biophys. Acta Bioenerg.* **767**, 548–556 (1984).
- M. Haumann, W. Junge, The rates of proton uptake and electron transfer at the reducing side of photosystem II in thylakoids. *FEBS Lett.* **347**, 45–50 (1994).
- I. Vass, Y. Inoue, pH dependent stabilization of S₂Q_A⁻ and S₂Q_B⁻ charge pairs studied by thermoluminescence. *Photosynth. Res.* **10**, 431–436 (1986).
- A. Krieger-Liszky, A. W. Rutherford, Influence of herbicide binding on the redox potential of the quinone acceptor in photosystem II: Relevance to photodamage and phototoxicity. *Biochemistry* **37**, 17339–17344 (1998).
- Z. Zhu, M. R. Gunner, Energetics of quinone-dependent electron and proton transfers in *Rhodobacter sphaeroides* photosynthetic reaction centers. *Biochemistry* **44**, 82–96 (2005).
- R. de Wijn, H. J. van Gorkom, Kinetics of electron transfer from Q_A to Q_B in photosystem II. *Biochemistry* **40**, 11912–11922 (2001).
- V. Petrouleas, A. R. Crofts, “The iron-quinone acceptor complex” in *Photosystem II*, T. Wydrzynski, K. Satoh, J. Freeman, Eds. (Springer-Verlag, Berlin, 2005), pp. 177–206.
- P. Pospíšil, Molecular mechanisms of production and scavenging of reactive oxygen species by photosystem II. *Biochim. Biophys. Acta Bioenerg.* **1817**, 218–231 (2012).
- J. H. Golbeck, B. Kok, Redox titration of electron acceptor Q and the plastoquinone pool in Photosystem II. *Biochim. Biophys. Acta Bioenerg.* **547**, 347–360 (1979).
- P. R. Rich, D. S. Bendall, The kinetics and thermodynamics of the reduction of cytochrome c by substituted p-benzoquinols in solution. *Biochim. Biophys. Acta Bioenerg.* **592**, 506–518 (1980).
- M. R. Gunner, J. Madeo, Z. Zhu, Modification of quinone electrochemistry by the proteins in the biological electron transfer chains: Examples from photosynthetic reaction centers. *J. Bioenerg. Biomembr.* **40**, 509–519 (2008).
- B. A. Diner, C. C. Schenck, C. De Vitry, Effect of inhibitors, redox state and isoprenoid chain length on the affinity of ubiquinone for the secondary acceptor binding site in the reaction centers of photosynthetic bacteria. *Biochim. Biophys. Acta Bioenerg.* **766**, 9–20 (1984).
- M. S. Graige, G. Feher, M. Y. Okamura, Conformational gating of the electron transfer reaction Q_A⁻Q_B → Q_AQ_B⁻ in bacterial reaction centers of *Rhodobacter sphaeroides* determined by a driving force assay. *Proc. Natl. Acad. Sci. U.S.A.* **95**, 11679–11684 (1998).
- J. Kern et al., Purification, characterisation and crystallisation of photosystem II from *Thermosynechococcus elongatus* cultivated in a new type of photobioreactor. *Biochim. Biophys. Acta Bioenerg.* **1706**, 147–157 (2005).
- R. Krivanek, J. Kern, A. Zouni, H. Dau, M. Haumann, Spare quinones in the QB cavity of crystallized photosystem II from *Thermosynechococcus elongatus*. *Biochim. Biophys. Acta Bioenerg.* **1767**, 520–527 (2007).
- M. Sugiura, Y. Inoue, Highly purified thermo-stable oxygen-evolving photosystem II core complex from the thermophilic cyanobacterium *Synechococcus elongatus* having His-tagged CP43. *Plant Cell Physiol.* **40**, 1219–1231 (1999).
- P. L. Dutton, Oxidation-reduction potential dependence of the interaction of cytochromes, bacteriochlorophyll and carotenoids at 77° K in chromatophores of Chromatium D and *Rhodospseudomonas gelatinosa*. *Biochim. Biophys. Acta* **226**, 63–80 (1971).
- S. De Causmaecker, “Bioenergetic studies on the quinone electron acceptors of photosystem II,” PhD thesis, Imperial College London, London, UK (2018).
- Y. Umena, K. Kawakami, J.-R. Shen, N. Kamiya, Crystal structure of oxygen-evolving photosystem II at a resolution of 1.9 Å. *Nature* **473**, 55–60 (2011).
- G. N. Johnson, A. Boussac, A. W. Rutherford, The origin of 40–50°C thermoluminescence bands in Photosystem II. *Biochim. Biophys. Acta Bioenerg.* **1184**, 85–92 (1994).
- Y. Kato, M. Sugiura, A. Oda, T. Watanabe, Spectroelectrochemical determination of the redox potential of pheophytin a, the primary electron acceptor in photosystem II. *Proc. Natl. Acad. Sci. U.S.A.* **106**, 17365–17370 (2009).